Brian D. Eldredge
University of Illinois at Urbana-Champaign,
158 MEB, MC-244,
1206 West Green Street,
Urbana, IL 61801
e-mail: brian.eldredge@gmail.com

Bryan P. Rasmussen
Texas A&M University,
3123 TAMU,
College Station, TX 77843-3123
e-mail: brasmussen@tamu.edu

Andrew G. Alleyne
University of Illinois at Urbana-Champaign,
158 MEB, MC-244,
1206 West Green Street,
Urbana, IL 61801
e-mail: alleyne@illinois.edu

Moving-Boundary Heat Exchanger Models With Variable Outlet Phase

Vapor compression cycle systems using accumulators and receivers inherently operate at or near a transition point involving changes of phase at the heat exchanger outlets. This work introduces a condenser/receiver model and an evaporator/accumulator model developed in the moving-boundary framework. These models use a novel extension of physical variable definitions to account for variations in refrigerant exit phase. System-level model validation results, which demonstrate the validity of the new models, are presented. The model accuracy is improved by recognizing the sensitivity of the models to refrigerant mass flow rate. The approach developed and the validated models provide a valuable tool for dynamic analysis and control design for vapor compression cycle systems. [DOI: 10.1115/1.2977466]

Keywords: thermo-fluid systems, dynamic models, vapor compression cycle

1 Introduction

Control engineers are often faced with the challenging task of creating simplified dynamic models of complex physical systems. A thermofluid system is a good example of a complex physical system that requires an accurate yet simple dynamic model for control design purposes. In this work, we present a thermofluid system dynamic model with specific application to vapor compression cycle (VCC) systems. New models are derived for heat exchangers used in conjunction with two common components: receivers and accumulators. The modeling approach balances the trade-offs between complexity and accuracy, arriving at a tool that is useful for both dynamic analysis and control design.

Modeling of VCC systems can be divided into two general paradigms: finite difference (spatially dependent) models and moving-boundary models [1]. In the finite difference paradigm, the conservation equations are approximated with a finite difference technique and applied to a number of elements in the heat exchanger [2]. Each element contains its own dynamic states and is independent of fluid phase. As the number of elements increases, model accuracy increases as well. However, the increased number of elements results in a dynamically complex model that may be computationally expensive and is unsuitable for model-based control design [3].

In the moving-boundary modeling approach, the heat exchangers are divided into regions based on the fluid phase in each region. Model parameters are lumped together in each region. The location of the boundary between regions is allowed to be a dynamic variable, thereby capturing the essential two-phase flow dynamics. The resulting models are of low dynamic order, making them very well suited for control design. The moving-boundary models give the model developer and control designer physical insight into the dynamic behavior of the plant. In comparison to the finite difference models, the compact nature of the moving-boundary models is assumed to reduce accuracy, although no direct model validation comparison is available in the literature. Grald and MacArthur showed that a spatially dependent model and a moving-boundary model for an evaporator have very similar dynamic responses [4].

Moving-boundary models have been under development since 1979 [5]. A review of the literature shows that they have been applied to a variety of VCC systems with many variations in the details of the modeling approach [1]. The range of operating conditions covered by many system models [5–9] has been limited by the lack of models for system components frequently used in practice, such as receivers and accumulators. Under normal operating conditions, heat exchangers used in conjunction with these components will experience changing fluid phase conditions at the heat exchanger outlet. In the established moving-boundary framework, these changing fluid phase conditions would result in the creation and destruction of dynamic states. Previous works [5,8] used a model switching approach to accommodate multiple modeling frameworks in one simulation. A key contribution of Willatzen et al. [8] is a presentation of techniques for controlling inactive states. The evaporator model is given in [8] as an example of the approach. Four model structures are considered: a subcool/two-phase/superheat model, a subcool/two-phase model, a two-phase model, and a two-phase/superheat model. The models are implemented with explicit equations for the state derivatives, allowing for direct manipulation of the derivatives. Two guiding principles are presented for handling state derivatives when the physical entities that they represent are not active in the model. First, if a state going to zero will adversely affect numerics, do not allow the state to reach zero. Second, force inactive states to track a meaningful physical value. The value to be tracked is determined by the desired state value at the time of its activation in the model. An evaporator switching from a subcool/two-phase/superheat model to a two-phase/superheat model provides an example of the application of these principles. As the model structure switch occurs, the subcooled region length goes to zero and the subcooled region wall temperature state becomes inactive. The model structure switching is based on the inlet and outlet refrigerant enthalpies. If, in the case of the evaporator, the inlet enthalpy is less than the saturated liquid enthalpy, the subcooled region is included. If the outlet enthalpy is greater than the saturated vapor enthalpy, the superheat region is included. No model validation results are presented in [8], but simulation results are presented for a number of model outputs.

The current work seeks to address the problem of multiple exit states without using a switching or multiple model approach. The rest of the paper is organized as follows. The modeling challenge associated with varying exit phase is addressed in Sec. 2 through the first-principles derivation of unique integrated condenser/

Contributed by the Dynamic Systems, Measurement, and Control Division of ASME for publication in the JOURNAL OF DYNAMIC SYSTEMS, MEASUREMENT, AND CONTROL. Manuscript received June 8, 2006; final manuscript received May 22, 2008; published online September 24, 2008. Assoc. Editor: Huei Peng.

receiver and evaporator/accumulator models. Section 2 expands the range of operating conditions that may be modeled with the moving-boundary framework. Section 3 provides model validation results demonstrating the utility of the proposed approach. The accuracy of the model validation in Sec. 3 is enhanced by an identified dynamic model of the compressor mass flow. The procedure and the model for the compressor are detailed in the Appendix. A conclusion summarizes the main points of the paper.

2 Moving-Boundary Models With Variable Outlet Phase

2.1 Moving-Boundary Heat Exchanger Model Overview. The moving-boundary approach is based on the assumption of one-dimensional fluid flow through a pipe with effective diameter, effective flow length, and effective surface areas [5–9]. The approach also assumes equal pressure throughout the heat exchanger. The heat exchanger is divided into regions based on the fluid phase, and the effective parameters are lumped in each region. The interface location between fluid phase regions is allowed to be a dynamic variable. Model parameters in single phase regions are the averages of the region's inlet and outlet conditions. Model parameters in the two-phase region are characterized by a mean void fraction [10]. For two-phase refrigerant flowing through a tube, the void fraction gives the ratio of area occupied by vapor to the total area at a cross section of the tube. Because two-phase flow is characterized by saturated conditions, the lumped parameters for the heat exchanger's two-phase region may be found by taking an average of the saturated vapor and the saturated liquid conditions. The mean void fraction, as detailed in Sec. 2.4.8, is used as the weight in this parameter averaging.

The moving-boundary derivation procedure requires the integration of the governing partial differential equations (PDEs) along the length of the heat exchanger to remove spatial dependence. The PDEs for conservation of refrigerant mass and energy are given in Eqs. (1) and (2). The z-coordinate specifies a location along the length of the heat exchanger. The inlet of the heat exchanger is described by $z=0$ and the outlet by $z=L_T$.

$$\frac{\partial(\rho A_{cs})}{\partial t} + \frac{\partial(\dot{m})}{\partial z} = 0 \tag{1}$$

$$\frac{\partial(\rho A_{cs} h - A_{cs} P)}{\partial t} + \frac{\partial(\dot{m} h)}{\partial z} = p_i \alpha_i (T_w - T_r) \tag{2}$$

Equation (1) is the differential continuity equation for unidirectional flow in the z direction. Equation (2) is the differential conservation of energy equation for the refrigerant in the heat exchanger, which states that the rate of energy change in the refrigerant due to changes in enthalpy, pressure, and position must equal the rate of heat transfer between the refrigerant and the heat exchanger wall.

The differential conservation of energy equation for the heat exchanger wall energy is given in Eq. (3). This equation shows that the rate of energy change in the wall due to temperature change must equal the rate of heat transfer between the wall and both the refrigerant and the surrounding air. The PDEs are integrated using the Leibniz integration rule given in Eq. (4). The conservation of momentum equation is neglected by assuming a uniform pressure along the length of the heat exchanger [6–9].

$$(C_p \rho A)_w \frac{\partial(T_w)}{\partial t} = p_i \alpha_i (T_r - T_w) + p_o \alpha_o (T_a - T_w) \tag{3}$$

$$\int_{z_1(t)}^{z_2(t)} \frac{\partial f(z,t)}{\partial t} dz = \frac{d}{dt}\left[\int_{z_1(t)}^{z_2(t)} f(z,t) dz\right] - f(z_2(t),t)\frac{d(z_2(t))}{dt} + f(z_1(t),t)\frac{d(z_1(t))}{dt} \tag{4}$$

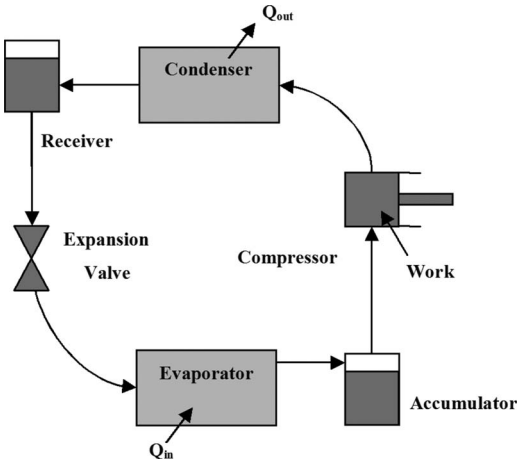

Fig. 1 A basic vapor compression cycle with a receiver and an accumulator

This modeling approach has been applied to both evaporators and condensers operating in subcritical and transcritical vapor compression cycle systems [6,11]. The resulting models were shown to be of low dynamic order and suitable for control design purposes.

2.2 Receivers and Accumulators in the Moving-Boundary Framework. A basic vapor compression cycle is composed of four primary components: evaporator, compressor, condenser, and expansion valve, as shown in Fig. 1. A high side receiver and/or low side accumulator is/are generally added to the system as a means of storing excess refrigerant and ensuring safe operation over a large range of operating conditions. From the condenser, the refrigerant flows to a receiver where any excess charge is stored. The refrigerant leaving the evaporator flows to an accumulator where any two-phase fluid is captured, thus preventing damage to the compressor.

The main challenge presented by the presence of receivers and accumulators is the possibility of multiple fluid phase conditions at the heat exchanger outlet. At steady-state conditions, a condenser with receiver will operate with saturated liquid or two-phase fluid at the outlet, as shown in Fig. 2. During transients, the condenser outlet fluid condition could deviate to subcooled outlet conditions, as shown in Fig. 3. Similarly, if an accumulator contains some liquid refrigerant, the evaporator will operate with saturated vapor or two-phase fluid at the outlet. Transients could cause the evaporator outlet fluid condition to deviate to superheated vapor conditions.

The creation of a subcooled region in the condenser or a superheated region in the evaporator presents the problem of the creation of new dynamic states, as fluid region lengths and wall

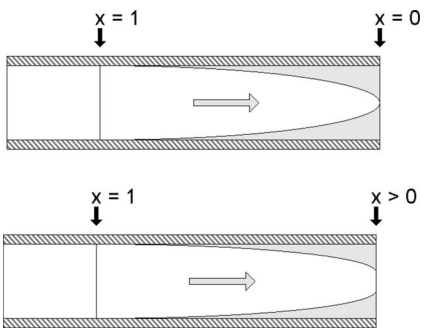

Fig. 2 Two possible steady-state operating conditions for a condenser with receiver

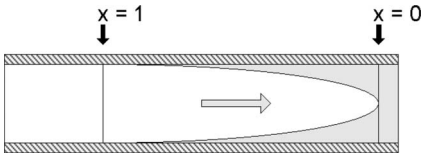

Fig. 3 A possible transient operating condition for a condenser with receiver

temperatures are states in the moving-boundary framework. When the system transients die out, the models face the problem of disappearing states. In the established moving-boundary framework, multiple model structures would be needed to capture the dynamics of heat exchangers operating with the possibility of multiple fluid phase conditions at the outlet [8]. In the following model derivations, we propose an extended definition of quality to capture the transient behavior of heat exchangers with receivers/accumulators and avoid the complications of switching model structures during simulation. Using this approach, the governing equations of the model do not require direct manipulation during simulation, regardless of the refrigerant phase at the heat exchanger outlet.

2.3 Receiver/Accumulator Model Derivation. High side receivers provide a volume for storing excess refrigerant charge and ensuring liquid flow into the expansion device. Low side accumulators protect compressors from "slugging" by capturing two-phase refrigerant and allowing only vapor to exit the accumulator and enter the compressor. For modeling purposes, the two components differ only in their inlet and outlet conditions. The receiver/accumulator is modeled as a simple control volume with refrigerant entering and exiting the control volume boundary. Heat transfer may occur between the walls of the receiver/accumulator and the surroundings. For the receiver, the entering refrigerant is either two-phase, saturated liquid, or subcooled liquid, and the exiting refrigerant is assumed to be saturated liquid, as shown in Fig. 4. The receiver pressure is assumed to be the condenser pressure. For the accumulator, the entering refrigerant is either two-phase, saturated vapor, or superheated vapor, and the exiting fluid is assumed to be saturated vapor, as shown in Fig. 5. The accumulator pressure is assumed to be the evaporator pressure.

The conservation of mass and energy for the receiver are written as Eqs. (5) and (6). Equation (5) shows that the rate of mass storage in the receiver is simply the net mass flow rate into the receiver. Equation (6) shows that the rate of change of refrigerant energy stored in the receiver is based on the energy entering and leaving the receiver due to mass flow and the heat transfer with the surroundings.

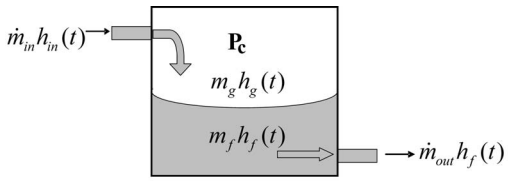

Fig. 4 Control volume for receiver model

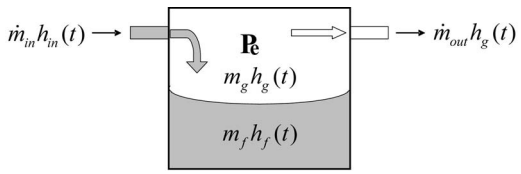

Fig. 5 Control volume for accumulator model

$$\frac{dm_{\text{rec}}}{dt} = \dot{m}_{\text{in}} - \dot{m}_{\text{out}} \tag{5}$$

$$\frac{d(m_{\text{rec}}u_{\text{rec}})}{dt} = \dot{m}_{\text{in}}h_{\text{in}} - \dot{m}_{\text{out}}h_{\text{out}} + UA(T_{\text{amb}} - T_{\text{rec}}) \tag{6}$$

The total refrigerant mass in the receiver is the summation of the liquid and vapor mass, $m_{\text{rec}}=m_g+m_f$. The total refrigerant energy is the summation of liquid and vapor energy, $m_{\text{rec}}u_{rec}=m_g u_g+m_f u_f$. The total volume of the receiver is the summation of liquid and vapor volumes, $V_{\text{rec}}=V_g+V_f$. The relationship between mass and volume is defined as $m_g=\rho_g V_g$ and $m_f=\rho_f V_f$. Using these relationships, the volume of each phase may be found in terms of the total mass and total volume as $V_g=(\rho_f V_{\text{rec}}-m_{\text{rec}})/(\rho_f-\rho_g)$ and $V_f=(\rho_g V_{\text{rec}}-m_{\text{rec}})/(\rho_g-\rho_f)$. The net change in volume is zero, $\dot{V}_g+\dot{V}_f=0$. By applying the chain rule of differentiation to the left hand side of Eq. (5), we find this expression for the receiver mass derivative:

$$\frac{dm_{\text{rec}}}{dt} = \frac{d(\rho_g V_g + \rho_f V_f)}{dt} = \frac{d(\rho_g)}{dt}V_g + \frac{d(\rho_f)}{dt}V_f + \rho_g\frac{d(V_g)}{dt} + \rho_f\frac{d(V_f)}{dt}$$
$$= \left[\frac{\partial(\rho_g)}{\partial P_c}V_g + \frac{\partial(\rho_f)}{\partial P_c}V_f\right]\dot{P}_c + [\rho_g - \rho_f]\dot{V}_g \tag{7}$$

Taking the same approach for the left hand side of Eq. (6) gives the receiver energy derivative:

$$\frac{d(m_{\text{rec}}u_{\text{rec}})}{dt} = \frac{d(\rho_g u_g V_g + \rho_f u_f V_f)}{dt} = \frac{d(\rho_g u_g)}{dt}V_g + \frac{d(\rho_f u_f)}{dt}V_f$$
$$+ \rho_g u_g\frac{d(V_g)}{dt} + \rho_f u_f\frac{d(V_f)}{dt}$$
$$= \left[\frac{\partial(\rho_g u_g)}{\partial P_c}V_g + \frac{\partial(\rho_f u_f)}{\partial P_c}V_f\right]\dot{P}_c + [\rho_g u_g - \rho_f u_f]\dot{V}_g \tag{8}$$

Again, we assume the receiver/accumulator pressure to be equal to that of the upstream heat exchanger. Combining these results allows us to write the conservation of refrigerant energy equation in terms of $\dot{m}_{\text{rec}}$ and $\dot{P}_c$, as shown in Eq. (9). Thus Eqs. (5) and (9) form the governing differential equations for the receiver.

$$\left[\left(\frac{d\rho_g}{dP_c}V_g u_g + \frac{d\rho_f}{dP_c}V_f u_f + \frac{du_g}{dP_c}\rho_g V_g + \frac{du_f}{dP_c}\rho_f V_f\right) - \left(\frac{\rho_g u_g - \rho_f u_f}{\rho_g - \rho_f}\right)\right.$$
$$\left.\times\left(\frac{d\rho_g}{dP_c}V_g + \frac{d\rho_f}{dP_c}V_f\right)\right]\dot{P}_c + \left[\frac{\rho_g u_g - \rho_f u_f}{\rho_g - \rho_f}\right]\dot{m}_{\text{rec}}$$
$$= \dot{m}_{\text{in}}h_{\text{in}} - \dot{m}_{\text{out}}h_{\text{out}} + UA_{\text{rec}}(T_{\text{amb}} - T_{\text{rec}}) \tag{9}$$

The equations for the accumulator are obtained by replacing the receiver terms with accumulator terms and the condenser terms with evaporator terms.

2.4 Condenser With Receiver Model Derivation. Nominally, the condenser is assumed to have two fluid regions (superheat and two-phase), as shown in Fig. 2. The derivation here follows the method presented in [11]. The starting point is the governing PDEs for mass and energy, Eqs. (1) and (2). We first remove the spatial dependence from the PDEs by integrating along the length of the pipe. The limits of integration depend on the fluid region. The conservation of mass and conservation of energy equations are first applied to the superheat region and then to the two-phase region. The conservation of energy equation is also applied to the pipe wall for each region.

2.4.1 Conservation of Mass: Superheat Region. Equation (1) for the conservation of mass is repeated here as the starting point of the derivation:

$$\frac{\partial(\rho A_{cs})}{\partial t} + \frac{\partial(\dot{m})}{\partial z} = 0 \tag{10}$$

Integrate the first term of Eq. (10) from the inlet of the pipe ($z=0$) to the end of the superheat region ($z=L_1$) and assume a constant cross-sectional area:

$$\int_0^{L_1} \frac{\partial(\rho A_{cs})}{\partial t} dz = A_{cs}\left[\int_0^{L_1} \frac{\partial(\rho)}{\partial t} dz\right] \tag{11}$$

Apply Leibniz's integration rule, Eq. (4):

$$\int_0^{L_1} \frac{\partial(\rho A_{cs})}{\partial t} dz = A_{cs}\left[\frac{d}{dt}\left(\int_0^{L_1} \frac{\partial(\rho)}{\partial t} dz\right) - \rho_g \dot{L}_1\right] \tag{12}$$

Assume a lumped density ρ_1 and evaluate the integral. During simulation this density will be calculated as the average of the condenser inlet density and the saturated vapor density at the condenser pressure.

$$\int_0^{L_1} \frac{\partial(\rho A_{cs})}{\partial t} dz = A_{cs}\left[\frac{d}{dt}(\rho_1 L_1) - \rho_g \dot{L}_1\right] \tag{13}$$

Evaluate the time derivative:

$$\int_0^{L_1} \frac{\partial(\rho A_{cs})}{\partial t} dz = A_{cs}[\dot{\rho}_1 L_1 + \rho_1 \dot{L}_1 - \rho_g \dot{L}_1] \tag{14}$$

Pressure and enthalpy are chosen as independent variables, and we assume a lumped enthalpy (h_1) that is an average of the enthalpies at the limits of integration. The derivatives of the superheat region enthalpy and density are given in Eqs. (16) and (17).

$$h_1 = \frac{h_{in} + h_g}{2} \tag{15}$$

$$\dot{h}_1 = \frac{1}{2}\left(\dot{h}_{in} + \frac{dh_g}{dP_c}\dot{P}_c\right) \tag{16}$$

$$\dot{\rho}_1 = \frac{\partial \rho_1}{\partial P_c}\dot{P}_c + \frac{\partial \rho_1}{\partial h_1}\dot{h}_1 \tag{17}$$

Substitute Eq. (16) into Eq. (17) to obtain

$$\dot{\rho}_1 = \frac{\partial \rho_1}{\partial P_c}\dot{P}_c + \frac{\partial \rho_1}{\partial h_1}\left[\frac{1}{2}\left(\dot{h}_{in} + \frac{dh_g}{dP_c}\dot{P}_c\right)\right] \tag{18}$$

Substitute Eq. (18) into Eq. (14):

$$\int_0^{L_1} \frac{\partial(\rho A_{cs})}{\partial t} dz = A_{cs}\left(\frac{\partial \rho_1}{\partial P_c}\dot{P}_c + \frac{\partial \rho_1}{\partial h_1}\left[\frac{1}{2}\left(\dot{h}_{in} + \frac{dh_g}{dP_c}\dot{P}_c\right)\right]\right)L_1 + (\rho_1 - \rho_g)\dot{L}_1 \tag{19}$$

Simplify to obtain

$$\int_0^{L_1} \frac{\partial(\rho A_{cs})}{\partial t} dz = \left(\frac{\partial \rho_1}{\partial P_c} + \frac{1}{2}\frac{\partial \rho_1}{\partial h_1}\frac{\partial h_g}{\partial P_c}\right)A_{cs}L_1\dot{P}_c + \left(\frac{1}{2}\frac{\partial \rho_1}{\partial h_1}\right)A_{cs}L_1\dot{h}_{in} + (\rho_1 - \rho_g)A_{cs}\dot{L}_1 \tag{20}$$

Integrate the second term of Eq. (10), defining the mass flow rate at the interface between the superheat region and the two-phase region as $\dot{m}_{int}$:

$$\int_0^{L_1} \frac{\partial \dot{m}}{\partial z} dz = \dot{m}_{int} - \dot{m}_{in} \tag{21}$$

Combining Eqs. (20) and (21) gives the desired conservation of mass equation for the superheat region.

$$\left(\frac{\partial \rho_1}{\partial P_c} + \frac{1}{2}\frac{\partial \rho_1}{\partial h_1}\frac{dh_g}{dP_c}\right)A_{cs}L_1\dot{P}_c + \left(\frac{1}{2}\frac{\partial \rho_1}{\partial h_1}\right)A_{cs}L_1\dot{h}_{in} + (\rho_1 - \rho_g)A_{cs}\dot{L}_1 = \dot{m}_{in} - \dot{m}_{int} \tag{22}$$

2.4.2 Conservation of Energy: Superheat Region. Begin with Eq. (2), repeated here as

$$\frac{\partial(\rho A_{cs} h)}{\partial t} - \frac{\partial(A_{cs} P_c)}{\partial t} + \frac{\partial(\dot{m} h)}{\partial z} = p_i \alpha_i (T_w - T_r) \tag{23}$$

Integrating the first term of Eq. (23) along the length of the superheat region and applying Eq. (4) yields

$$\int_0^{L_1} \frac{\partial(\rho A_{cs} h)}{\partial t} dz = \frac{d}{dt}\int_0^{L_1} (\rho A_{cs} h) dz - \rho_g A_{cs} h_g \dot{L}_1 \tag{24}$$

Again assuming a lumped density and enthalpy, evaluate the integral and the time derivative.

$$\int_0^{L_1} \frac{\partial(\rho A_{cs} h)}{\partial t} dz = A_{cs}[\dot{\rho}_1 h_1 L_1 + \rho_1 \dot{h}_1 L_1 + \rho_1 h_1 \dot{L}_1 - \rho_g h_g \dot{L}_1] \tag{25}$$

Substitute Eq. (18) and Eq. (16) into Eq. (25) and simplify to obtain the first term of Eq. (23).

$$\int_0^{L_1} \frac{\partial(\rho A_{cs} h)}{\partial t} dz = \left(\left(\frac{\partial \rho_1}{\partial P_c}\dot{P}_c + \frac{1}{2}\frac{\partial \rho_1}{\partial h_1}\frac{\partial h_g}{\partial P_c}\right)h_1 + \frac{1}{2}\frac{\partial h_g}{\partial P_c}\rho_1\right)A_{cs}L_1\dot{P}_c + \left(\frac{1}{2}\frac{\partial \rho_1}{\partial h_1}h_1 + \frac{1}{2}\rho_1\right)A_{cs}L_1\dot{h}_{in} + (\rho_1 h_1 - \rho_g h_g)A_{cs}\dot{L}_1 \tag{26}$$

The second term of Eq. (23) is integrated with the same limits. Applying Eq. (4) again and evaluating the integral yields

$$\int_0^{L_1} \frac{\partial(A_{cs} P_c)}{\partial t} dz = A_{cs}\left[\frac{d}{dt}(P_c L_1) - P_c \dot{L}_1\right] \tag{27}$$

Evaluate the time derivative and simplify

$$\int_0^{L_1} \frac{\partial(A_{cs} P_c)}{\partial t} dz = A_{cs}\dot{P}_c L_1 \tag{28}$$

Integrate the third term of Eq. (23). At the interface between regions, the mass flow rate is $\dot{m}_{int}$, and the enthalpy is the saturated vapor enthalpy.

$$\int_0^{L_1} \frac{\partial(\dot{m} h)}{\partial z} dz = \dot{m}_{int} h_g - \dot{m}_{in} h_{in} \tag{29}$$

Now combine Eqs. (26), (28), and (29) with Eq. (23) and simplify to find the final conservation of energy equation for the superheat region.

$$\left[\left(\frac{\partial \rho_1}{\partial P_c} + \frac{1}{2}\frac{\partial \rho_1}{\partial h_1}\frac{dh_g}{dP_c}\right)h_1 + \left(\frac{1}{2}\frac{dh_g}{dP_c}\right)\rho_1 - 1\right]A_{cs}L_1\dot{P}_c + \left[\left(\frac{1}{2}\frac{\partial \rho_1}{\partial h_1}\right)h_1 + \left(\frac{1}{2}\right)\rho_1\right]A_{cs}L_1\dot{h}_{in} + (\rho_1 h_1 - \rho_g h_g)A_{cs}\dot{L}_1 = \dot{m}_{in} h_{in} - \dot{m}_{int} h_g + \alpha_{i1} A_i \left(\frac{L_1}{L_T}\right)(T_{w1} - T_{r1}) \tag{30}$$

2.4.3 Conservation of Refrigerant Mass: Two-Phase Region. Integrate the first term of Eq. (10) from the beginning of the two-phase region ($z=L_1$) to the end of the pipe ($z=L_T$) and apply Eq. (4).

$$\int_{L_1}^{L_T} \frac{\partial(\rho A_{cs})}{\partial t} dz = A_{cs}\left[\frac{d}{dt}\int_{L_1}^{L_T} (\rho) dz + \rho_g \dot{L}_1\right] \tag{31}$$

Assume that the lumped density can be evaluated as a function of the void fraction and evaluate the integral.

$$\int_{L_1}^{L_T} \frac{\partial(\rho A_{cs})}{\partial t} dz = A_{cs}\left[\frac{d}{dt}((\rho_f(1-\bar{\gamma}) + \rho_g(\bar{\gamma}))(L_T - L_1)) + \rho_g \dot{L}_1\right] \tag{32}$$

Evaluate the time derivative, treating enthalpies as functions of pressure.

$$\int_{L_1}^{L_T} \frac{\partial(\rho A_{cs})}{\partial t} dz = \left(\frac{d\rho_f}{dP_c}(1-\bar{\gamma}) + \frac{d\rho_g}{dP_c}(\bar{\gamma})\right) A_{cs}\dot{P}_c(L_T - L_1) + (\rho_g - \rho_f) \times (\dot{\bar{\gamma}}) A_{cs}(L_T - L_1) + (\rho_g - \rho_f(1-\bar{\gamma}) - \rho_g(\bar{\gamma})) A_{cs}\dot{L}_1 \tag{33}$$

Note that $L_T - L_1 = L_2$. Integrate the second term of Eq. (10) and combine the result with Eq. (33) to find the conservation of mass equation for the two-phase region.

$$(\rho_g - \rho_f)(1-\bar{\gamma}) A_{cs}\dot{L}_1 + \left(\frac{d\rho_f}{dP_c}(1-\bar{\gamma}) + \frac{d\rho_g}{dP_c}(\bar{\gamma})\right) A_{cs}L_2\dot{P}_c + (\rho_g - \rho_f) A_{cs}L_2\dot{\bar{\gamma}} = \dot{m}_{int} - \dot{m}_{out} \tag{34}$$

2.4.4 Conservation of Refrigerant Energy: Two-Phase Region. Beginning with Eq. (23), integrate the first term and apply Eq. (4).

$$\int_{L_1}^{L_T} \frac{\partial(\rho A_{cs} h)}{\partial t} dz = A_{cs}\left[\frac{d}{dt}\int_{L_1}^{L_T} (\rho h) dz + \rho_g h_g \dot{L}_1\right] \tag{35}$$

Assume that density and enthalpy can be expressed in terms of the void fraction and evaluate the integral.

$$\int_{L_1}^{L_T} \frac{\partial(\rho A_{cs} h)}{\partial t} dz = A_{cs}\left[\frac{d}{dt}(\rho_f h_f(1-\bar{\gamma})L_2 + \rho_g h_g(\bar{\gamma})L_2) + \rho_g h_g \dot{L}_1\right] \tag{36}$$

Assume that the enthalpy and density are functions of pressure. The time derivative is then evaluated.

$$\int_{L_1}^{L_T} \frac{\partial(\rho A_{cs} h)}{\partial t} dz = A_{cs}\left[\left(\frac{\partial\rho_f}{\partial P_c} h_f(1-\bar{\gamma})L_2 + \frac{\partial h_f}{\partial P_c}\rho_f(1-\bar{\gamma})L_2 + \frac{\partial\rho_g}{\partial P_c} h_g \bar{\gamma} L_2 + \frac{\partial h_g}{\partial P_c}\rho_g \bar{\gamma} L_2\right)\dot{P}_c + (\rho_g h_g - \rho_g h_g(\bar{\gamma}) - \rho_f h_f(1-\bar{\gamma}))\dot{L}_1 + \left(\rho_g h_g L_2 - \rho_f h_f L_2\right)\dot{\bar{\gamma}}\right] \tag{37}$$

Integrate the second term of Eq. (23) by applying Eq. (4) and assuming a constant pressure:

$$\int_{L_1}^{L_T} \frac{\partial(A_{cs}P_c)}{\partial t} dz = A_{cs}\left[\frac{d}{dt}(P_c L_T - P_c L_1) + P_c \dot{L}_1\right] \tag{38}$$

Evaluate the time derivative:

$$\int_{L_1}^{L_T} \frac{\partial(A_{cs}P_c)}{\partial t} dz = A_{cs}\dot{P}_c(L_T - L_1) \tag{39}$$

Evaluate the final term of Eq. (23):

$$\int_{L_1}^{L_T} \frac{\partial(\dot{m}h)}{\partial z} dz = \dot{m}_{out}h_{out} - \dot{m}_{int}h_{int} \tag{40}$$

Combine Eqs. (37), (39), and (40) to obtain the conservation of energy equation for the two-phase region.

$$(\rho_g h_g - \rho_f h_f)(1-\bar{\gamma}) A_{cs}\dot{L}_1 + (\rho_g h_g - \rho_f h_f) A_{cs}L_2\dot{\bar{\gamma}} + \left(\frac{d(\rho_f h_f)}{dP_c}(1-\bar{\gamma}) + \frac{d(\rho_g h_g)}{dP_c}(\bar{\gamma}) - 1\right) A_{cs}L_2\dot{P}_c = \dot{m}_{int}h_g - \dot{m}_{out}h_{out} + \alpha_{i2}A_i\left(\frac{L_2}{L_T}\right)(T_{w2} - T_{r2}) \tag{41}$$

2.4.5 Conservation of Pipe Wall Energy: Superheat Region. Application of Eq. (3) to the superheat region wall gives

$$(C_P\rho V)_w\left(\dot{T}_{w1} + \frac{T_{w1} - T_{w2}}{L_1}\dot{L}_1\right) = \alpha_{i1}A_i(T_{r1} - T_{w1}) + \alpha_o A_o(T_a - T_{w1}) \tag{42}$$

2.4.6 Conservation of Pipe Wall Energy: Two-Phase Region. Application of Eq. (3) to the two-phase region wall gives

$$(C_P\rho V)_w\dot{T}_{w2} = \alpha_{i2}A_i(T_{r2} - T_{w2}) + \alpha_o A_o(T_a - T_{w2}) \tag{43}$$

2.4.7 Combination of Equations. Equations (22), (30), (34), and (41) together with Eqs. (5) and (9) from the receiver derivation are combined to eliminate the variables $\dot{m}_{int}$, $\dot{m}_{out}$ of the condenser, and $\dot{m}_{in}$ of the receiver, resulting in a model with six states: $x_c = [L_1\ P_c\ m_{rec}\ \bar{\gamma}\ T_{w1}\ T_{w2}]^T$. The model inputs are defined as $u_c = [\dot{m}_{c,in}\ \dot{m}_{rec,out}\ h_{c,in}\ T_{c,air,in}\ \dot{m}_{c,air}\ T_{amb}]^T$. The resulting model is given in Eq. (44) in descriptor form, $Z_c(x_c, u_c)\cdot\dot{x}_c = f_c(x_c, u_c)$, with the elements of the $Z_c(x_c, u_c)$ matrix found in Table 1.

$$\begin{bmatrix} z_{11} & z_{12} & 0 & 0 & 0 & 0 \\ z_{21} & z_{22} & z_{23} & z_{24} & 0 & 0 \\ z_{31} & z_{32} & z_{33} & z_{34} & 0 & 0 \\ 0 & z_{42} & 0 & z_{44} & 0 & 0 \\ z_{51} & 0 & 0 & 0 & z_{55} & 0 \\ 0 & 0 & 0 & 0 & 0 & z_{66} \end{bmatrix}\begin{bmatrix} \dot{L}_1 \\ \dot{P}_c \\ \dot{\bar{\gamma}} \\ \dot{m}_{rec} \\ \dot{T}_{w1} \\ \dot{T}_{w2} \end{bmatrix} = \begin{bmatrix} \dot{m}_{c,in}(h_{c,in} - h_g) + \alpha_{i1}A_i\left(\frac{L_1}{L_T}\right)(T_{w1} - T_{r1}) \\ \dot{m}_{rec,out}(h_g - h_{c,out}) + \alpha_{i2}A_i\left(\frac{L_2}{L_T}\right)(T_{w2} - T_{r2}) \\ \dot{m}_{c,in} - \dot{m}_{rec,out} \\ \dot{m}_{rec,out}(h_{c,out} - h_f) + UA_{rec}(T_{amb} - T_{rec}) \\ \alpha_{i1}A_i(T_{r1} - T_{w1}) + \alpha_o A_o(T_a - T_{w1}) \\ \alpha_{i2}A_i(T_{r2} - T_{w2}) + \alpha_o A_o(T_a - T_{w2}) \end{bmatrix} \tag{44}$$

In Eq. (44), the time derivative of condenser inlet enthalpy is sufficiently small so as to neglect it. This was found through numerical studies [11]. The model is simulated by calculating $\dot{x}_c = Z_c^{-1}f_c$ at each time step and numerically integrating to find the state vector x_c. This model structure can also be linearized locally to give a state space representation ($\dot{x}_c = A_c x_c + B_c u_c$) suitable for controller design. An actual controller design is beyond the scope of this paper, which focuses on modeling. The method of switching model structures during simulation [8] requires an explicit equation for each state derivative, so $Z_c^{-1}f_c$ must be evaluated symbolically. The model presented here is used throughout the simulation without modification, regardless of the outlet phase of

Table 1 Entries of Z_c (x_c, u_c) for the condenser with receiver model

z_{11}	$(\rho_1 h_1 - \rho_1 h_g) A_{cs}$
z_{12}	$\left[\left(\frac{\partial \rho_1}{\partial P_c} + \frac{1}{2}\frac{\partial \rho_1}{\partial h_1}\frac{dh_g}{dP_c}\right)(h_1 - h_g) + \left(\frac{1}{2}\frac{dh_g}{dP_c}\right)\rho_1 - 1\right] A_{cs} L_1$
z_{21}	$(\rho_f h_g - \rho_f h_f)(1-\bar{\gamma}) A_{cs}$
z_{22}	$\left(\frac{d(\rho_f h_f)}{dP_c}(1-\bar{\gamma}) + \frac{d(\rho_g h_g)}{dP_c}\bar{\gamma} - \frac{d\rho_f}{dP_c} h_g (1-\bar{\gamma}) - \frac{d\rho_g}{dP_c} h_g \bar{\gamma} - 1\right) A_{cs} L_2$
z_{23}	$(\rho_f h_g - \rho_f h_f) A_{cs} L_2$
z_{24}	$(h_{c,\text{out}} - h_g)$
z_{31}	$[\rho_1 - \rho_f(1-\bar{\gamma}) - \rho_g \bar{\gamma}] A_{cs}$
z_{32}	$\left[\left(\frac{d\rho_f}{dP_c}(1-\bar{\gamma}) + \frac{d\rho_g}{dP_c}\bar{\gamma}\right) L_2 + \left(\frac{\partial \rho_1}{\partial P_c} + \frac{1}{2}\frac{\partial \rho_1}{\partial h_1}\frac{dh_g}{dP_c}\right) L_1\right] A_{cs}$
z_{33}	$(\rho_g - \rho_f) A_{cs} L_2$
z_{34}	1
z_{42}	$\frac{d\rho_g}{dP_c} V_g u_g + \frac{d\rho_f}{dP_c} V_f u_f + m_g \frac{du_g}{dP_c} + m_f \frac{du_f}{dP_c} - \left(\frac{\rho_g u_g - \rho_f u_f}{\rho_g - \rho_f}\right)\left(\frac{d\rho_g}{dP_c} V_g + \frac{d\rho_f}{dP_c} V_f\right)$
z_{44}	$\left(\frac{\rho_g u_g - \rho_f u_f}{\rho_g - \rho_f} - h_{c,\text{out}}\right)$
z_{51}	$(C_p \rho V)_w \left(\frac{T_{w1} - T_{w2}}{L_1}\right)$
z_{55}	$(C_p \rho V)_w$
z_{66}	$(C_p \rho V)_w$

the condenser. No structural changes take place during simulation, so explicit equations for the state derivatives are not needed.

2.4.8 Condenser Outlet Quality From Mean Void Fraction. The mean void fraction, $\bar{\gamma}$, was chosen in the derivation as a dynamic state variable. The mean void fraction captures the relationship between vapor mass and liquid mass in the heat exchanger and is used in the calculation of lumped parameters in the two-phase region. We also use the mean void fraction to determine the outlet quality and hence the fluid properties at the outlet of the condenser. A slip-ratio (S) [12] void fraction correlation relates the void fraction to the quality at any point in the two phase region, as shown in Eq. (45) where $\mu_s = (\rho_g/\rho_f)S$. The slip ratio is the ratio of the vapor velocity to the liquid velocity. Numerous methods have been introduced for determining suitable values of S. The particular method does not impact this derivation.

$$\gamma = \frac{x}{x + (1-x)\mu_s} \tag{45}$$

From examination of Eq. (45), it is readily apparent that the limits on void fraction are the same as the limits on quality. As quality approaches zero, the void faction also approaches zero. As quality approaches 1, the void fraction approaches 1 as well.

The mean void fraction, Eq. (46), results from integrating Eq. (45) from x_{in} to x_{out} and dividing by $x_{\text{out}} - x_{\text{in}}$. This equation relates the mean void fraction to the inlet and outlet quality of the two-phase region. Once the outlet quality is obtained, all other outlet conditions may be calculated.

$$\bar{\gamma} = \frac{1}{(1-\mu_S)} + \frac{\mu_S}{(x_{\text{out}} - x_{\text{in}})(1-\mu_S)^2} \times \ln\left[\frac{\mu_S + x_{\text{in}}(1-\mu_S)}{\mu_S + x_{\text{in}}(1-\mu_S) + (x_{\text{out}} - x_{\text{in}})(1-\mu_S)}\right] \tag{46}$$

At steady-state, the inlet fluid of the condenser's two-phase region is saturated vapor ($x_{\text{in}}=1$) and the outlet fluid is saturated liquid ($x_{\text{out}}=0$) or two-phase liquid ($0 < x_{\text{out}} < 1$). We would like to use Eq. (46) to obtain the outlet quality for small deviations from saturated liquid conditions, but the equation is transcendental in outlet quality. Assuming small deviations from saturated liquid outlet conditions, we set $x_{\text{out}}=0$ outside of the natural log to arrive at Eq. (47). Solving for x_{out} yields Eq. (48), where $a = \mu_s/(1-\mu_s)$ and $b = 1/(1-\mu_s)$.

$$\bar{\gamma} \approx \frac{1}{1-\mu_s} - \frac{\mu_s}{(1-\mu_s)^2} \ln\left[\frac{1}{\mu_s + x_{\text{out}}(1-\mu_s)}\right]. \tag{47}$$

$$x_{\text{out}} = b e^{((\bar{\gamma} - b)/\text{ab})} - a \tag{48}$$

During simulation, some transients will cause the condenser's outlet fluid to deviate to subcooled conditions. When quality is calculated from the mean void fraction, Eq. (48), these deviations result in a quality value less than zero. We therefore define a pseudoquality that exists outside the normal bounds on quality, $x \in [0,1]$. This pseudoquality is defined as $\hat{x} \in [0-\varepsilon, 0) \cup (1, 1+\varepsilon)$, where $0 < \varepsilon \ll 1$. By using the two-phase property relationships with the pseudoquality, outlet refrigerant property approximations that capture the gross property behavior are obtained. The accuracy of the pseudoquality approximation will be discussed in Sec. 2.6.

2.5 Evaporator With Accumulator Model. When connected to an accumulator containing fluid in the liquid phase, the evaporator outlet condition is saturated vapor ($x_{\text{out}}=1$) or two-phase fluid ($0 < x_{\text{out}} < 1$) at equilibrium. The derivation of the evaporator model follows the method presented in [6], where the evaporator has a single two-phase region. This derivation is similar to the derivation of the condenser model and will not be presented in detail. The conservation of mass and conservation of energy equations are

$$\left(\frac{d\rho_f}{dP_e}(1-\bar{\gamma}) + \frac{d\rho_g}{dP_e}(\bar{\gamma})\right) A_{cs} L_T \dot{P}_e + (\rho_g - \rho_f) A_{cs} L_T \dot{\bar{\gamma}} = \dot{m}_{\text{in}} - \dot{m}_{\text{int}} \tag{49}$$

$$\left(\frac{d(\rho_f h_f)}{dP_e}(1-\bar{\gamma}) + \frac{d(\rho_g h_g)}{dP_e}(\bar{\gamma}) - 1\right) A_{cs} L_T \dot{P}_e + (\rho_g h_g - \rho_f h_f) A_{cs} L_T \dot{\bar{\gamma}} = \dot{m}_{\text{in}} h_{\text{in}} - \dot{m}_{\text{int}} h_{\text{int}} + \alpha_i A_i (T_w - T_r) \tag{50}$$

The conservation of energy equation for the evaporator wall is given by

$$(C_p \rho V)_w \dot{T}_w = \alpha_i A_i (T_r - T_w) + \alpha_o A_o (T_a - T_w) \tag{51}$$

Combining the evaporator equations with the equations for the accumulator results in a fourth-order model with states $x_e = [P_e \; m_{\text{acc}} \; \bar{\gamma} \; T_w]^T$ and inputs $u_e = [\dot{m}_{e,\text{in}} \; \dot{m}_{\text{acc,out}} \; h_{e,\text{in}} \; T_{e,\text{air,in}} \; \dot{m}_{e,\text{air}} \; T_{\text{amb}}]^T$. Writing the equations in descriptor form gives Eq. (52). The entries of $Z_e(x_e, u_e)$ are found in Table 2.

Table 2 Entries of $Z_e(x_e, u_e)$ for the evaporator with accumulator model

z_{11}	$\left[\left(\frac{d\rho_f}{dP_e}\right)(1-\bar{\gamma})+\left(\frac{d\rho_g}{dP_e}\right)\bar{\gamma}\right]A_{cs}L_T$
z_{12}	1
z_{13}	$(\rho_g-\rho_f)A_{cs}L_T$
z_{21}	$\left[\left(\frac{d(\rho_f h_f)}{dP_e}\right)(1-\bar{\gamma})+\left(\frac{d(\rho_g h_g)}{dP_e}\right)(\bar{\gamma})-1\right]A_{cs}L_T$
z_{22}	$h_{e,\text{out}}$
z_{23}	$(\rho_g h_g-\rho_f h_f)A_{cs}L_T$
z_{31}	$\left(\frac{d\rho_g}{dP_e}V_g u_g+\frac{d\rho_f}{dP_e}V_f u_f+\frac{du_g}{dP_e}\rho_g V_g+\frac{du_f}{dP_e}\rho_f V_f\right)$ $-\left(\frac{\rho_g u_g-\rho_f u_f}{\rho_g-\rho_f}\right)\left(\frac{d\rho_g}{dP_e}V_g+\frac{d\rho_f}{dP_e}V_f\right)$
z_{32}	$\left(\frac{\rho_g u_g-\rho_f u_f}{\rho_g-\rho_f}-h_{e,\text{out}}\right)$
z_{44}	$(C_p\rho V)_w$

$$\begin{bmatrix} z_{11} & z_{12} & z_{13} & 0 \\ z_{21} & z_{22} & z_{23} & 0 \\ z_{31} & z_{32} & 0 & 0 \\ 0 & 0 & 0 & z_{44} \end{bmatrix} \begin{bmatrix} \dot{P}_e \\ \dot{m}_{\text{acc}} \\ \dot{\bar{\gamma}} \\ \dot{T}_w \end{bmatrix} = \begin{bmatrix} \dot{m}_{e,\text{in}} - \dot{m}_{\text{acc,out}} \\ \dot{m}_{e,\text{in}} h_{e,\text{in}} - \dot{m}_{\text{acc,out}} h_g + \alpha_i A_i (T_w - T_r) \\ \dot{m}_{\text{acc,out}}(h_g - h_{e,\text{out}}) - UA_{\text{acc}}(T_{\text{acc}} - T_{\text{amb}}) \\ \alpha_i A_i (T_r - T_w) + \alpha_o A_o (T_a - T_w) \end{bmatrix} \quad (52)$$

2.5.1 Evaporator Outlet Quality From Mean Void Fraction. As with the condenser with receiver model, the mean void fraction is a dynamic state of the evaporator with accumulator model. Equation (46) again provides the means of relating mean void fraction to quality. We assume small deviations from saturated vapor outlet conditions, setting $x_{\text{out}}=1$ inside of the natural log to arrive at Eq. (53). Solving for x_{out} yields Eq. (54).

$$\bar{\gamma} \approx \frac{1}{1-\mu_s} + \frac{\mu_s}{(x_{\text{out}}-x_{\text{in}})(1-\mu_s)^2} \ln[\mu_s + x_{\text{in}}(1-\mu_s)] \quad (53)$$

$$x_{\text{out}} = \frac{\mu_S \ln[\mu_S + x_{\text{in}}(1-\mu_S)]}{(1-\mu_S)^2 \bar{\gamma} - (1-\mu_S)} + x_{\text{in}} \quad (54)$$

Outlet fluid properties are calculated from the two-phase property relationships using either the quality or the pseudo-quality.

2.6 Validity of the Mean Void Fraction Assumptions. By using the pseudoquality, the models capture the essential heat exchanger outlet refrigerant property behavior without the complications of switching model structures during simulation. This section addresses the validity of two key assumptions: the small deviation assumption used to derive Eqs. (47) and (54) and the assumption that approximate refrigerant properties calculated from the pseudoquality capture the basic behavior of the true refrigerant properties with sufficient accuracy for dynamic modeling purposes.

2.6.1 Small Deviation Assumption. Figure 6 compares the mean void fraction of Eq. (46) with the mean void fraction resulting from application of the condenser and evaporator small outlet quality deviation assumptions developed in Eqs. (47) and (54). In the case of the condenser, deviations over the range $x_{\text{out}} \in [0, 0.2]$ result in errors less than 3.5%. In the case of the evaporator, deviations over the range $x_{\text{out}} \in [0.8, 1]$ result in errors less than 1%. Therefore, under these normal simulation conditions, the small deviation assumptions applied to the mean void fraction do not produce significant errors. The small deviation assumptions should not be applied to other operating conditions, such as startup and shutdown transients where large deviations in heat exchanger outlet conditions are probable.

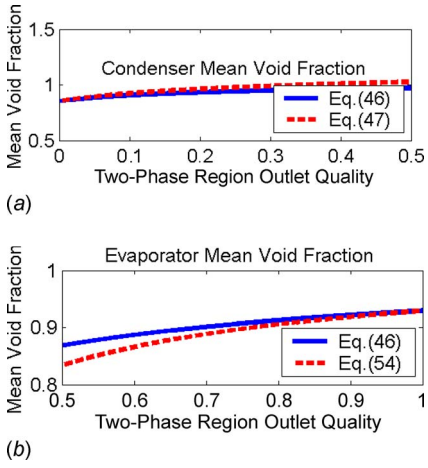

Fig. 6 Mean void fraction for two-phase flows operating at 900 kPa (condenser) and 320 kPa (evaporator) as a function of the outlet quality

2.6.2 Refrigerant Property Calculation. If a subcooled region develops in a condenser, the outlet enthalpy will decrease with the outlet temperature. Transitioning from quality to pseudoquality ($\hat{x}<0$) mimics the introduction of a subcooled region at the outlet of the condenser. Rather than create a new subcooled region and the associated states, the approximate outlet enthalpy is calculated as if the refrigerant were two-phase: $h=h_f(1-x)+h_g x$. The creation of a subcooled region in the real heat exchanger corresponds to an increase in liquid volume in the heat exchanger and therefore a lower mean void fraction across the two-phase and subcooled regions. As the subcooled region grows longer, the pseudoquality becomes more negative and the outlet enthalpy decreases. This decreasing pseudoquality results in a decreasing outlet enthalpy approximation, demonstrating that the properties calculated from the pseudoquality capture the key behavior of the true refrigerant properties. A similar argument could be made for the case of superheated outlet conditions in the evaporator. Using the pseudoquality allows the models to capture the essential transient behavior without using a model switching scheme.

For a numerical example, we consider the case of a condenser operating with a saturated liquid outlet condition. Assuming a slip ratio of 2 and a condenser pressure of 1000 kPa, the mean void fraction is 0.84 as calculated from Eq. (46). Using Eq. (48), we find that the outlet quality is approximately zero, which agrees with our initial assumption of a saturated liquid outlet condition. If the model's mean void fraction state increases above 0.84, the outlet refrigerant of the condenser will be two-phase. Now we extend our example to the case of a condenser with a subcooled region at the outlet. The concept of mean void fraction as a relative measure of liquid and vapor in the heat exchanger is applied to both the two-phase region and the subcooled region. With the subcooled region included, the mean void fraction will be less than 0.84. If the mean void fraction state in our example drops to 0.8, the pseudoquality calculated from Eq. (48) for the condenser

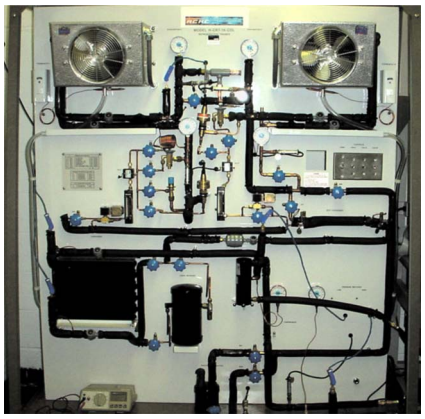

Fig. 7 Photograph of the experimental system

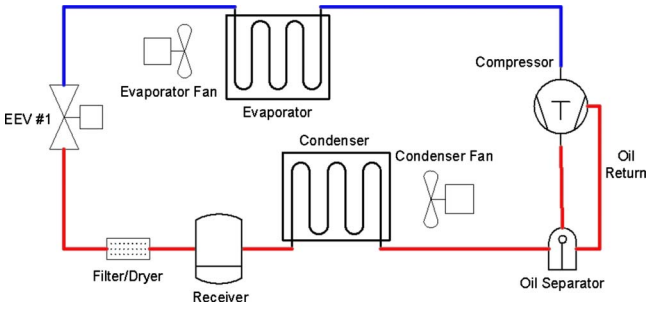

Fig. 8 Schematic of the experimental system

outlet is −0.03. The negative pseudoquality value results in an outlet enthalpy value less than the saturated liquid enthalpy.

3 Model Validation Results

3.1 Model Library. The moving-boundary models described in this paper are implemented in Thermosys, a MATLAB toolbox first described in [13]. Thermosys contains linear and nonlinear models of the basic components of VCC systems. The models of individual components may be used independently or combined with other components to create a complete system model. When a system is modeled, the inputs to each component model are generally the outputs of other component models. For example, the condenser model inputs include the inlet and outlet refrigerant mass flow rates. These mass flow rates are outputs of the compressor and valve models. Further details on the Thermosys toolbox are found in [13].

3.2 Experimental System. The experimental system used for validation is located at the Air Conditioning and Refrigeration Center at the University of Illinois at Urbana-Champaign. The main components are a $\frac{1}{2}$ horsepower variable speed compressor, a tube and fin condenser, two tube and fin evaporators, and four expansion devices. The system is instrumented with pressure transducers, mass flow meters, and thermocouples. For the model validation results presented here, the system is used in the single evaporator configuration with an electronic expansion valve. The high side receiver and low side accumulator are included in the

Table 3 Component physical parameters

Component	Parameter	Value	Units	Comments
Condenser	Heat exchanger mass	4.656	kg	Calculated
	Heat exchanger specific heat	0.467	kJ/kg K	Steel
	Heat exchanger frontal area	0.0898	m^2	From manufacturer
	Hydraulic diameter of tubes	0.008103	m	Measured
	Internal volume	0.00055716	m^3	From manufacturer
	Internal surface area	0.274993	m^2	Calculated
	External surface area	2.7927	m^2	Calculated
	Total fluid flow length	10.6895	m	Calculated
	Flow cross sectional area	0.00005156	m^2	Calculated
	Receiver volume	0.0007732	m^3	Measured
Evaporator 2	Heat exchanger mass	2.7438	kg	Calculated
	Heat exchanger specific heat	0.4877	kJ/kg K	Aluminum and copper
	Heat exchanger frontal area	0.0584	m^2	Calculated
	Hydraulic diameter of tubes	0.0081026	m	From manufacturer
	Internal volume	0.000591	m^3	From manufacturer
	Internal surface area	0.29166	m^2	Calculated
	External surface area	3.068	m^2	Calculated
	Total fluid flow length	11.45794	m	Calculated
	Flow cross sectional area	0.00005156	m^2	Calculated
	Accumulator volume	0.0028665	m^3	Measured
EEV	Rising slew rate	12.5	%/s	From manufacturer
	Falling slew rate	−12.5	%/s	From manufacturer
	Input delay	0.5	s	Estimated
Compressor	Volume	0.0000304	m^3	From manufacturer
	Rising slew rate	1000	rpm/s	Estimated
	Falling slew rate	−1000	rpm/s	Estimated
Pipe Length	Compressor to condenser	4.04	m	Measured
	Condenser to valve	4.79	m	Measured
	Valve to evaporator	1.63	m	Measured
	Evaporator to compressor	6.53	m	Measured
	Hydraulic diameter	9.5	mm	Estimated

Table 4 Model validation operating conditions

Evaporator	Units	Value
Pressure	kPa	273.1
Inlet enthalpy	kJ/kg	105.9
Outlet refrigerant temperature	°C	18.25
Refrigerant mass flow rate	kg/s	0.00713
Slip ratio		4.6
Inlet air temperature	°C	23.98
Outlet air temperature	°C	17.04
Air mass flow rate	kg/s	0.1568
Two-phase HTC	$kW/m^2 K$	2
Superheat HTC	$kW/m^2 K$	0.04
Air-side HTC 2 (from *j* factor)	$kW/m^2 K$	0.058
Compressor	**Units**	**Value**
Inlet pressure	kPa	263.5
Outlet pressure	kPa	975
Inlet temperature	°C	21.91
Outlet temperature	°C	64.42
Refrigerant mass flow rate	kg/s	0.00713
Compressor speed	rpm	1600
Condenser with receiver	**Units**	**Value**
Pressure	kPa	970
Inlet refrigerant temperature	°C	59.65
Refrigerant mass flow rate	kg/s	0.00713
Slip ratio		2.9
Inlet air temperature	°C	25.67
Outlet air temperature	°C	30.44
Air mass flow rate	kg/s	0.2938
Superheat HTC	$kW/m^2 K$	0.3879
Two-phase HTC	$kW/m^2 K$	1
Air-side HTC 2 (from *j* factor)	$kW/m^2 K$	0.126
Receiver refrigerant mass	kg	0.8
Receiver ambient temperature	°C	27
Electronic expansion valve	**Units**	**Value**
Inlet pressure	kPa	975
Outlet pressure	kPa	296.5
Inlet temperature	°C	37.13
Refrigerant mass flow rate	kg/s	0.00713
Input signal	%	13

system, necessitating the use of the new condenser with receiver model. The low side accumulator contains only vapor, so the evaporator with accumulator model is not needed. A photograph of the system is shown in Fig. 7. A schematic of the system in the model validation configuration is given in Fig. 8. The physical parameters of the experimental system components are given in Table 3. These parameters were obtained by measurement, by estimation, or from the component manufacturer. Operating conditions for this model validation scenario are shown in Table 4. Compressor and expansion valve mass flow rates are calculated from empirical performance maps. The refrigerant-side heat transfer coefficients are tuned parameters that remain the same throughout the simulation. Air-side heat transfer coefficients are calculated from *j*-factor correlations [14] and are updated during simulation.

3.3 Model Validation Results. The model validation test scenario consists of steps to each of the four controllable inputs: valve opening, compressor speed, evaporator air mass flow rate, and condenser air mass flow rate, as summarized in Table 5. The plots in Figs. 9–13 compare experimental data with various model outputs. It should be noted that the system configuration used here could not be accurately modeled without the condenser/receiver model presented in this paper. As encircled on Fig. 14, the condenser model's outlet quality briefly deviates to pseudoquality following the compressor speed step and the evaporator fan speed step at approximately 1430 s and 2200 s, respectively. This result indicates that the model predicted the formation of a subcooled

Table 5 Steps in system inputs

Input	Step time	Before step	After step	% of range
Valve open command	1000 s	13	14.5	9.4%
Compressor rpm	1400 s	1600 rpm	1800 rpm	14.3%
Cond. air mass flow	1800 s	0.2938 kg/s	0.2858 kg/s	2.7%
Evap. air mass flow	2200 s	0.1568 kg/s	0.1363 kg/s	13.1%

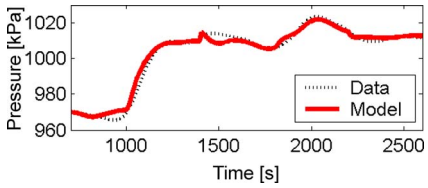

Fig. 9 Condenser pressure

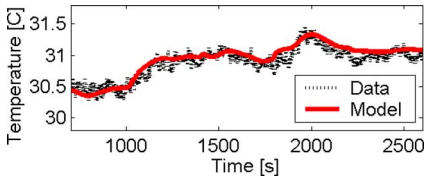

Fig. 10 Condenser air outlet temperature

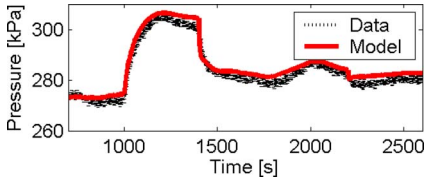

Fig. 11 Evaporator pressure

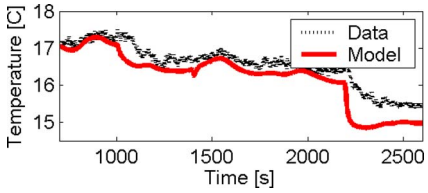

Fig. 12 Evaporator air outlet temperature

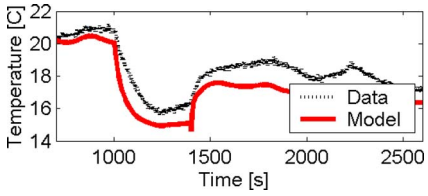

Fig. 13 Evaporator superheat

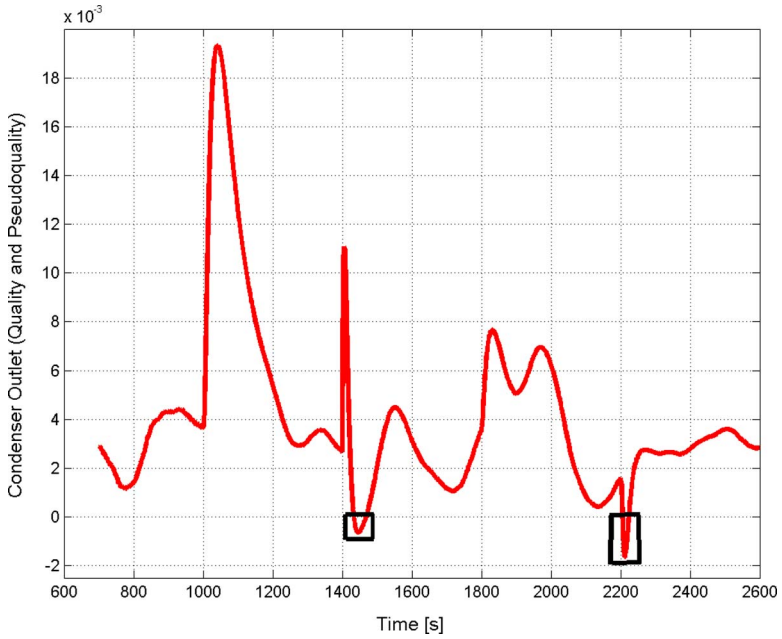

Fig. 14 Quality and pseudoquality calculated from the mean void fraction state

region at the condenser outlet. By using the pseudoquality, the model was able to capture this condition without interrupting the simulation to switch model structures.

4 Conclusions

New first-principles models are presented for heat exchangers used in conjunction with receivers and accumulators, including a detailed derivation of the condenser/receiver model. These models expand the range of operating conditions that may be modeled in the moving-boundary framework. By extending the definition of a key physical variable (quality), the models are able to accommodate fluctuations in outlet fluid phase conditions without switching model structure during simulation, thereby avoiding the creation and destruction of dynamic states. Model validation results are presented for a complete system model. The modeled experimental system contains a receiver, necessitating the use of the new model presented here. The results demonstrate that the moving-boundary models are capable of representing systems with receivers and accumulators.

The validation results indicate that the low-order nonlinear moving-boundary models are potentially a useful tool for dynamic analysis of VCC systems. The nonlinear models may be linearized to provide models that are sufficiently accurate and compact to serve as tools for model-based control design. Future research will focus on further improvements to model accuracy and application of the models as a control design tool.

Acknowledgment

The authors wish to thank the sponsoring companies of the Air Conditioning and Refrigeration Center for their financial support of this work. Mike Keir was instrumental in preparing the experimental system used to generate the model validation data.

Nomenclature

Symbol

A = area
C_p = specific heat
L = length
P = pressure
Q = heat transfer rate
S = slip ratio
T = temperature
UA = product of area and overall heat transfer coefficient
V = volume
Z = descriptor form matrix
e = error
h = enthalpy
m = mass
sh = superheat
t = time
u = internal energy, inputs vector
x = quality, states vector
$\hat{x}$ = pseudoquality
z = spatial coordinate
γ = void fraction
$\hat{\gamma}$ = mean void fraction
α = heat transfer coefficient, weighting factor
Δ = change
η = efficiency
ρ = density
ω = angular velocity

Subscripts

1 = fluid region 1
2 = fluid region 2
a = air
acc = accumulator
amb = ambient
c = condenser
cs = cross-sectional
e = evaporator
f = saturated fluid
g = saturated vapor
i = inner
in = in to control volume
int = fluid region interface
k = compressor
k = iteration

k–tot = compressor, total
o = outer
out = out of control volume
r = refrigerant
rec = receiver
T = total
vol = volumetric
w = wall

Appendix: Dynamic Compressor Mass Flow Models

1 Static Compressor Mass Flow Model

The heat exchanger models presented in Sec. 2 are known to be very sensitive to inlet and outlet refrigerant mass flow rates [15]. To improve the modeling accuracy, a dynamic compressor mass flow rate model was incorporated and used for the validation results of Sec. 3. The reader should note that this Appendix is not necessary for the correctness of the models presented in Sec. 2. However, it was found to greatly impact the accuracy of the comparison between simulation and data in Sec. 3. Therefore, it is included here for completeness.

The modeling of compressors in VCC systems can be categorized in two broad groups: simple static models [6,7,9] and complex dynamic models [5,16]. The simplified static models rely on time scale separation; the compressor dynamics are much faster than the heat exchanger dynamics, and therefore the compressor dynamics are treated as if they were instantaneous [11]. A static compressor model typically uses a semi-empirical modeling approach. The compressor mass flow rate is given by Eq. (A1), where V_k is the cylinder volume, ω_k is the compressor speed, and ρ_k is the inlet refrigerant density [6].

$$\dot{m}_k = \omega_k V_k \rho_k \eta_{\text{vol}} \tag{A1}$$

During simulation, the volumetric efficiency, η_{vol}, is found from a performance map generated through extensive compressor testing.

The performance map is generated by first solving Eq. (A1) for the volumetric efficiency. By modulating the compressor speed and valve opening settings, the experimental system is run over the feasible range of inlet and outlet compressor pressures. The changes in compressor speed and valve opening are sufficiently slow that each instance of the test can be considered a nearly steady-state operating condition. Using measurements of mass flow rate, compressor speed, and inlet density, the volumetric efficiency is calculated. Performance map indices are chosen as compressor speed and pressure ratio across the compressor. An equation with these inputs is fitted to the volumetric efficiency data with a least-squares linear regression. An example of a performance map generated in this fashion is shown in Fig. 15. The performance map, together with Eq. (A1), constitutes a semi-empirical static compressor model.

2 Dynamic Mass Flow Model

The first step in the identification of the dynamic mass flow rate model is the isolation of the mass flow dynamics from a complete system simulation. The static semi-empirical compressor model presented in Sec. A.1 provides the base line mass flow model. An iterative learning control (ILC) algorithm [17,18] is used to identify a mass flow rate correction. The ILC algorithm adjusts the mass flow rate to reduce the error in one of the outputs, in this case the evaporator pressure. Figure 16 shows a schematic of the isolation procedure.

The base line static compressor model produces a mass flow rate prediction that is used to simulate a particular cycle. After the simulation has finished, the evaporator pressure model output is compared to evaporator pressure data to generate an evaporator pressure error signal. This error signal is passed to the *PD*-type ILC algorithm given in Eq. (A2), where P and D are tunable gains on the evaporator pressure error and pressure error derivative, k is the iteration number, and trial is the data length.

$$\dot{m}(t)_{\text{correction},k} = \dot{m}(t)_{\text{correction},k-1} + P \cdot e(t)_{k-1} + D \cdot \dot{e}(t)_{k-1}, \quad t \in [0,\text{trial}] \tag{A2}$$

The ILC algorithm produces a feed-forward mass flow rate correction signal that is applied to the mass flow rate predicted by the static compressor model during the next iteration of the simulation. Iterations continue until the rms evaporator pressure error reaches an acceptably small value. At the final iteration, the mass flow rate correction signal represents an isolation of the mass flow rate dynamics not captured by the static model.

After isolation of the mass flow dynamics, a model is identified to capture the dynamic behavior. First-, second-, and third-order models were identified using standard techniques and compared. The model identification was carried out using the MATLAB Sys-

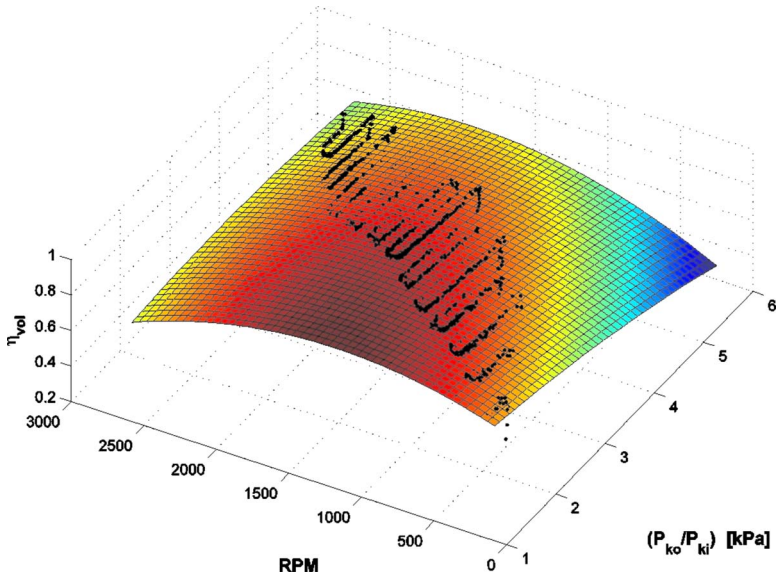

Fig. 15 A compressor volumetric efficiency performance map showing experimentally obtained data (black points) and a least-squares fit surface modeling the data

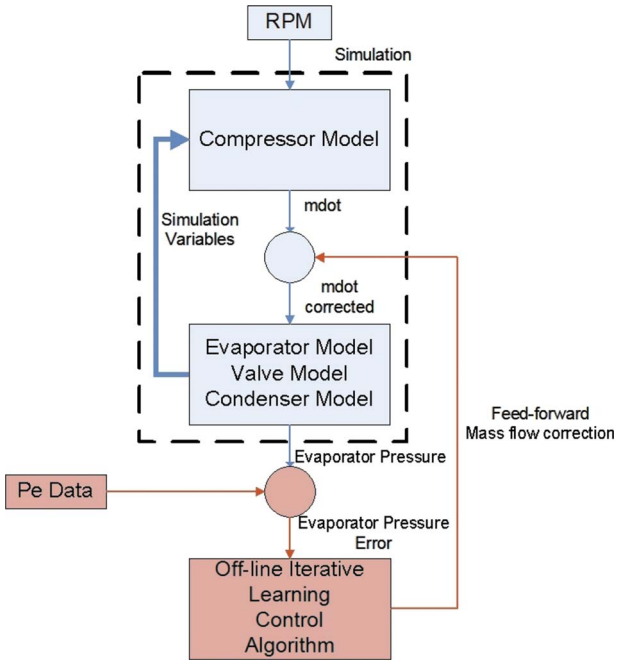

Fig. 16 Schematic of the mass flow dynamics isolation procedure

tem Identification Toolbox. The model structure is the linear time-invariant output error model described in [19]. A first order model was chosen as a desirable trade-off between accuracy and simplicity since its accuracy was similar to higher order models [15]. The model inputs are the deviations from the initial conditions of the compressor inlet pressure, outlet pressure, and speed. The mass flow correction model is of the form given in Eq. (A3), where $G_{\Delta P_{\text{in}}}$, $G_{\Delta P_{\text{out}}}$, and $G_{\Delta\omega_k}$ are the identified transfer functions defined in Eqs. (A4)–(A6)

$$\dot{m}_{\text{correction}} = \begin{bmatrix} G_{\Delta P_{\text{in}}} & G_{\Delta P_{\text{out}}} & G_{\Delta\omega_k} \end{bmatrix} \begin{bmatrix} \Delta P_{\text{in}} \\ \Delta P_{\text{out}} \\ \Delta\omega_k \end{bmatrix} \tag{A3}$$

$$G_{\Delta P_{\text{in}}} = \frac{8.698 \times 10^{-7} s + 9.014 \times 10^{-7}}{s + 0.07181} \tag{A4}$$

$$G_{\Delta P_{\text{out}}} = \frac{-4.893 \times 10^{-8} s - 4.923 \times 10^{-8}}{s + 0.01232} \tag{A5}$$

$$G_{\Delta\omega_k} = \frac{1.591 \times 10^{-7} s + 1.659 \times 10^{-7}}{s + 0.08469} \tag{A6}$$

The total compressor mass flow is then given as

$$\dot{m}_{k\_\text{tot}} = \dot{m}_k + \dot{m}_{\text{correction}} \tag{A7}$$

References

[1] Bendapudi, S., and Braun, J. E., 2002, "A Review of Literature on Dynamic Models of Vapor Compression Equipment," ASHRAE Report No. 4036-5.

[2] MacArthur, J. W., and Grald, E. W., 1989, "Unsteady Compressible Two-Phase Flow Model for Predicting Cyclic Heat Pump Performance and a Comparison With Experimental Data," Int. J. Refrig., **12**(1), pp. 29–41.

[3] Anderson, B. D. O., 1993, "Controller Design: Moving From Theory to Practice," IEEE Control Syst. Mag., **13**(4), pp. 16–25.

[4] Grald, E. W., and MacArthur, J. W., 1992, "A Moving-Boundary Formulation for Modeling Time-Dependent Two-Phase Flows," Int. J. Heat Fluid Flow, **13**(3), pp. 266–272.

[5] Dhar, M., and Soedel, W., 1979, "Transient Analysis of a Vapor Compression Refrigeration System," *Proceedings of the 15th International Congress of Refrigeration*, Venice, Sept. 23–29, Vol. 2, pp. 1031–1067.

[6] Rasmussen, B. P., and Alleyne, A. G., 2004, "Control-Oriented Modeling of Transcritical Vapor Compression Systems," ASME J. Dyn. Syst., Meas., Control, **126**, pp. 54–64.

[7] He, X. D., Asada, H., Liu, S., and Itoh, H., 1998, "Multivariable Control of Vapor Compression Systems," HVAC&R Res., **4**(3), pp. 205–230.

[8] Willatzen, M., Pettit, N. B. O. L., and Ploug-Sorensen, L., 1998, "General Dynamic Simulation Model for Evaporators and Condensers in Refrigeration. Part I: Moving-Boundary Formulation of Two-Phase Flows With Heat Exchange," Int. J. Refrig., **21**(5), pp. 398–403.

[9] Jensen, J. M., and Tummescheit, H., 2002, "Moving-Boundary Models for Dynamic Simulations of Two-Phase Flows," *Proceedings of the Second International Modelica Conference*, Oberpfaffenhofen, Germany, March 18–19, pp. 235–244.

[10] Wedekind, G. L., Bhatt, B. L., and Beck, B. T., 1978, "A System Mean Void Fraction Model for Predicting Various Transient Phenomena Associated With Two-Phase Evaporating and Condensing Flows," Int. J. Multiphase Flow, **4**(1), pp. 97–114.

[11] Rasmussen, B. P., 2005, "Dynamic Modeling and Advanced Control of Air Conditioning and Refrigerating Systems," Ph.D. thesis, University of Illinois at Urbana-Champaign, Urbana.

[12] Rice, C. K., 1987, "Effect of Void Fraction Correlation and Heat Flux Assumption on Refrigerant Charge Inventory Predictions," ASHRAE Trans., **93**(1), pp. 341–376.

[13] Rasmussen, B. P., 2000, "Control-Oriented Modeling of Transcritical Vapor Compression Systems," MS thesis, University of Illinois at Urbana-Champaign, Urbana.

[14] Kays, W. M., and London, A. L., 1984, *Compact Heat Exchangers*, McGraw-Hill, Inc., New York.

[15] Eldredge, B., Rasmussen, B., and Alleyne, A., 2006, "Automotive Vapor Compression Cycles: Validation of Control-Oriented Models," *Proceedings of 2006 SAE World Congress*, Detroit, April 3–6, SAE Technical Paper No. 2006-01-1452.

[16] Chi, J., and Didion, D. A., 1982, "A Simulation Model of the Transient Performance of a Heat Pump," Int. J. Refrig., **5**(3), pp. 176–184.

[17] Moore, K. L., 1993, *Iterative Learning Control for Deterministic Systems*, Springer-Verlag, London, pp. 9–22.

[18] Bristow, D. A., Tharayil, M., and Alleyne, A., 2006, "A Survey of Iterative Learning Control: A Learning-Based Method for High-Performance Tracking Control," IEEE Control Syst., **26**(3), pp. 96–114.

[19] Ljung, L., 1999, *System Identification*, Prentice-Hall, Englewood Cliffs, NJ.